Ease-off based compensation of tooth surface deviations for spiral bevel and hypoid gears: only the pinion needs corrections

Alessio Artoni[a,*], Marco Gabiccini[a], Mohsen Kolivand[b]

[a] *Dipartimento di Ingegneria Meccanica, Nucleare e della Produzione, University of Pisa, Largo Lucio Lazzarino 2, 56122 Pisa, Italy*
[b] *American Axle & Manufacturing Inc., 2965 Technology Dr, Rochester Hills, MI 48309, USA*

Abstract

This paper presents a novel methodology to restore the designed functional properties of hypoid gear sets whose teeth deviate from their theoretical models due to inevitable imperfections in the machining process. Corrective actions are applied to one member only: the pinion. The concept of ease-off is profitably employed as the true means to evaluate the contact properties of a gear set as a whole. It is indeed the sameness of the designed and the real ease-off that ultimately renders two gear sets equivalent in terms of contact pattern, transmission error and vibrational properties. On this basis, gear deviations can be mapped into equivalent pinion deviations, added to those of the pinion itself, and cumulatively compensated for by applying corrective machine-tool settings to the pinion. The gear member is perfect "as is". The ensuing advantages are highlighted in the paper. The method is illustrated with a real-life numerical example. It demonstrates that, applying corrective (i) machine-tool settings and (ii) machine settings only to the pinion grinding process, the originally designed transmission properties can be restored with a high level of accuracy.

Keywords: hypoid gears, spiral bevel gears, correction, surface deviations, surface errors, ease-off

*Corresponding author. Tel.: +39 050 2218020. Fax: +39 050 2218065
Email addresses: alessio.artoni@ing.unipi.it (Alessio Artoni), m.gabiccini@ing.unipi.it (Marco Gabiccini), mohsen.kolivand@aam.com (Mohsen Kolivand)

1. Introduction and literature review

The tooth surfaces of real cut/ground spiral bevel and hypoid gears inevitably deviate from their theoretical models due to a number of error sources inherent in hypoid generators. Design tolerances and systematic inaccuracies in tool geometry and machine settings, machine flexibility and consequent deformation during cutting, and dynamic effects are the key culprits in tooth surface errors. Additional distortions are induced by the heat treatment processes used for tooth surface hardening.

Despite their magnitude, typically a few dozen microns, tooth surface deviations generally have detrimental effects on contact properties, especially in terms of contact pattern quality and transmission error amplitude. This is due to the fact that the tooth surfaces of spiral bevel and hypoid gears are nearly conjugate, hence very sensitive to micro-geometry variations. For these reasons, researchers have been dedicating a lot of efforts to determining appropriate correction strategies for the problem at hand. Eventually, the problem boils down to *identifying the machine-tool setting corrections* required to compensate for the deviations between real teeth and their designed, theoretical counterparts. A chronological literature review follows. All studies (including the present one) are based on the assumption that the inherent errors of a certain hypoid generator are systematic and repeatable.

One of the first studies on corrective machine settings was published by Krenzer [1, 2]. His procedure approximated the error surface as a quadratic one and then corrected the first and second order terms in two subsequent stages by linear regression. Litvin et al. gave an analytical formulation of the inspection process with coordinate measuring machines in [3], where minimization of tooth surface deviations was framed as a nonlinear optimization problem for the first time. Corrections based on a linear relationship between gear surface and machine settings were proposed by Litvin et al. in [4]. A method similar to the one in [2] was presented by Stadtfeld in [5, ch. 9], while an approach based on linear regression and similar to the one in [4] was presented by Lin et al. in [6], together with a sensitivity analysis of tooth surface to machine-tool setting variations. Gosselin et al. [7] defined five average surface errors and minimized them by eventually solving a nonlinear system of five equations in five unknown machine settings. Lin et al. [8] applied nonlinear optimization techniques to find corrective settings. They employed the multifunctional optimization system tool, based on the SQP method, to minimize a cost function defined as the maximum tooth surface deviation. Shih and Fong in [9] presented a method to identify the corrective settings of six-axis CNC hypoid generators (as opposed to the classic cradle-style generators)

through application of linear regression. Artoni et al. in [10] proposed a nonlinear least squares formulation for the problem of identifying the machine-tool settings needed to generate a target ease-off topography. The choice of solving it by a trust-region Levenberg-Marquardt method allowed to easily cope with the ubiquitous problem of ill-conditioning, arising from near dependencies between machine-tool settings. This aspect is critical when a large number of them are selected as design variables, especially in association with particularly demanding surface topographies. In [11, 12], Fan et al. presented a closed-loop correction process based on the iterative application of linear regression to determine corrective universal motion coefficients. A discussion about the effects of different definitions of tooth surface deviations and flank referencing procedures is provided by Guenther in [13]. Finally, in their recent paper [14], Gabiccini et al. made a comparative analysis of the above-listed methods and introduced the concepts of eigen-topographies and eigen-corrections, by which target surface topographies can be easily classified according to their practical reachability.

In modern industrial practice, actual tooth surfaces are probed by coordinate measuring machines (CMM) at a predefined number of points, and their deviations from the nominal points are measured along the directions of the local normal vectors. Usually, three or four teeth are inspected, and their deviations averaged. Tooth thickness, whose accuracy is particularly important for proper backlash, is measured at a specified reference point, and its deviation is stored in angular units. (Somewhat surprisingly, the above-listed works, with the exception of [13], do not explicitly discuss tooth thickness deviation, and its correction is briefly mentioned in just a few cases.) A typical so-called *closed-loop* correction process involves the following basic steps (see, e.g., [11]).

1. Special software (e.g., Gleason CAGE or Klingelnberg KIMoS) is used to generate nominal data for the pinion and the gear under inspection.
2. Pinion and gear are cut/ground using their basic machine-tool settings, then they are sent to the CMM, where they are measured.
3. If the deviations between measured and nominal data exceed tolerances, special programs (e.g., Gleason G-AGE or Klingelnberg KOMET) are used to calculate corrective machine-tool settings for the two mating members.
4. Pinion and gear are remachined using the calculated corrective settings, then they are measured by the CMM.

In certain cases, the last two steps may need to be applied several times until the tolerance requirements are met.

The present paper proposes a novel correction method, based on the fact that contact properties are chiefly determined by the so-called *ease-off topography*. Therefore, a correction mechanism is successful if it can reestablish the designed, theoretical ease-off topography. As will be detailed in the next sections, this fact has the convenient and remarkable consequence that gear deviations can be mapped into equivalent pinion deviations and added to the original pinion deviations, thus defining cumulative pinion deviations. As a result, the gear member is "perfect as is", while calculation of machine-tool setting corrections and subsequent corrective machining, aimed at compensating for such cumulative deviations, have to be conducted *for the pinion only*, with significant advantages in terms of cost and time savings. Corrective machine-tool setting variations are calculated by solving a properly formulated nonlinear least squares problem. The proposed method also includes *tooth thickness correction*. The level of accuracy that can be attained is expected to be *at least* the same as that of the methods currently in use. All advantages of this method are summarized in the Conclusions section.

2. Definition of ease-off

The study presented in this paper is based on the fact that contact properties—the *macro*-geometry being fixed—are primarily determined by the designed *micro*-geometry, in particular by the ease-off topography of the mating tooth flanks. Ease-off comprises all sorts of tooth flank modifications (profile crown, lead crown, flank twist, and higher-order crown) applied to both the pinion and the gear tooth surfaces, and it also accounts for the presence of misalignments. In other terms, it measures the extent by which the meshing tooth surfaces of pinion and gear depart from conjugacy. While it is rather intuitive that ease-off dictates the contact properties of the mating flanks (in particular, size and location of the contact pattern, contact pressures, motion transmission errors, and their sensitivity to misalignments), this fact was quantitatively demonstrated by Kolivand and Kahraman in [15, 16].

The terms "ease-off" and "ease-off topography" are often used as synonyms. Strictly speaking, while the former stands for the ease-off value calculated at a generic point on the tooth surface, the latter should denote the set of ease-off values calculated at a number of points, usually arranged as a grid on a specific area of the tooth surface (the potential contact area, as we shall see).

Before going into the details of the proposed correction method, let us take a closer look at the operations and tools involved in the definition of ease-off and required to

calculate it.

2.1. Relative position between pinion and gear

The first step to defining ease-off is to establish a relative position between the pinion and the gear. Is is important to clarify right off that ease-off depends on such relative position. Therefore, ease-off is designed (and defined) for a specific relative position—it could be termed *design point* position—that is generally the one in which the two members spend the most part of their service life.

Figure 1 details the geometric parameters used to specify the relative position between the pinion and the gear and the assembly errors (or misalignments), along with their sign conventions based on the Gleason system set-up. Pinion and gear are represented by their pitch cones. It is worth recalling in passing that, unlike spiral bevel

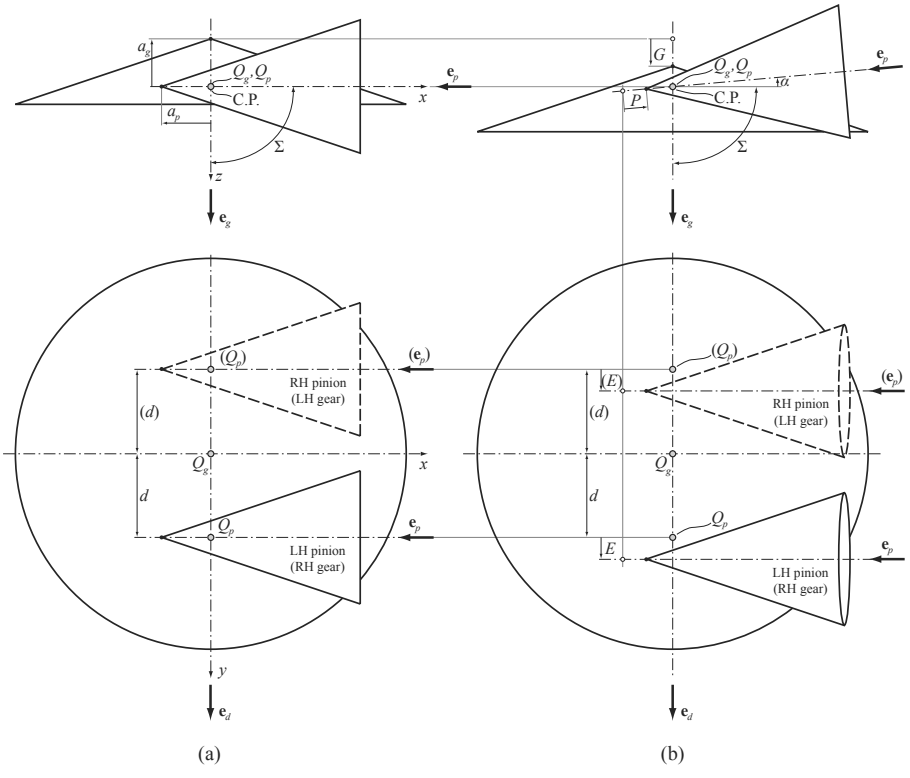

Figure 1: Pitch cones expressing the general relative position between hypoid pinion and gear. (Here, the common 90-degree shaft angle layout is depicted.) Relevant parameters (a) in the nominal position and (b) in the presence of misalignments.

gears, pitch cones of hypoid gears *are not* their axodes (which are circular hyperboloids).

The symbols in Fig. 1 represent the following quantities (terminology details can be found in [17]).

- Σ is the shaft angle.
- d is the hypoid offset.
- The assembly errors E, P, G, and α are the offset error, pinion axial error, gear axial error, and shaft angle error, respectively.
- The unit vector $\boldsymbol{e}_p$ ($\boldsymbol{e}_g$) marks the pinion (gear) axis.
- With zero offset error E, point Q_p (Q_g) is the point of intersection between the pinion (gear) axis and the line of the shortest distance between the two axes (direction of offset, marked by the unit vector $\boldsymbol{e}_d = \boldsymbol{e}_p \times \boldsymbol{e}_g$). When the two points Q_p and Q_g are looked at from the direction of such line, they coalesce into the crossing point C.P., illustrated in the upper part of Fig. 1. Q_p and Q_g will be considered *fixed points* in the following.

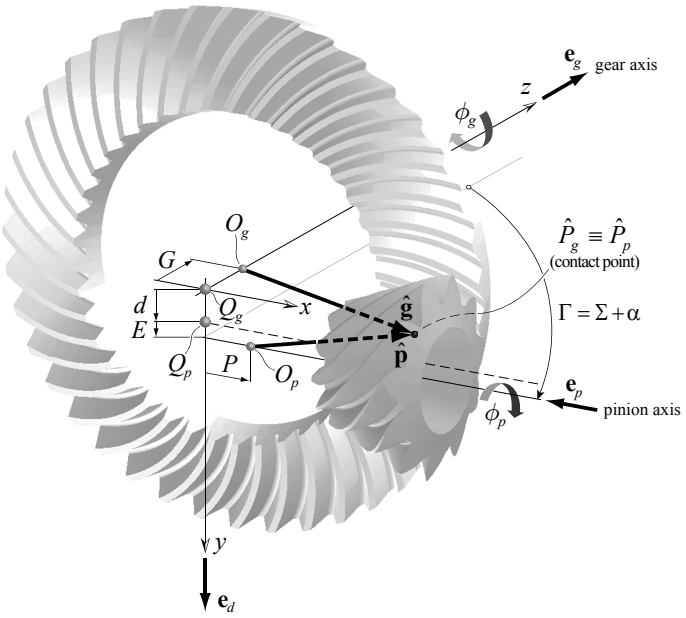

Figure 2: General relative position between hypoid pinion and gear. Case of left-hand pinion and right-hand gear.

- a_p (a_g) is the so-called pinion (gear) pitch apex beyond crossing point.

A 3D representation of the scenario in Fig. 1 is provided in Fig. 2, which will be detailed later. Such a general relative position, including the presence of misalignments, will be considered in the following.

2.2. Equation of meshing and conjugate surfaces

The well-known *equation of meshing* (see, e.g., [18, pp. 98-99] or [19, pp. 618-621]), also known as *conjugacy equation* [16, p. 2], is a fundamental tool for ease-off calculation. It is required to determine the pinion surface that would be conjugate to the given (nominal) gear tooth surface, or the gear surface that would be conjugate to the given (nominal) pinion tooth surface.

Let us set out to obtain the conjugate pinion tooth surface. In particular, we will be considering the conjugate pinion point generated by a generic point of the gear tooth surface (e.g., on the drive side), represented by its position vector $\boldsymbol{g}$ and its local unit normal $\boldsymbol{n}_g$.

With reference to Fig. 2, the origins of the local position vectors $\boldsymbol{p}$ and $\boldsymbol{g}$, representing the pinion and gear tooth surfaces, coincide with the fixed points Q_p and Q_g, respectively, when the gear drive is perfectly aligned. As a consequence of misalignment, the pinion body is displaced by E, P and α, and the gear body by G. The fixed points O_p and O_g are the images of Q_p and Q_g as a result of misalignment. The hatted vectors $\hat{\boldsymbol{p}}$ and $\hat{\boldsymbol{g}}$ shown in Fig. 2 denote the images of vectors $\boldsymbol{p}$ and $\boldsymbol{g}$ after they have performed rotations about their respective (pinion and gear) axes, according to

$$\hat{\boldsymbol{p}}(\phi_p) = R(\boldsymbol{p}, \boldsymbol{e}_p, \phi_p) \tag{1}$$

$$\hat{\boldsymbol{g}}(\phi_g) = R(\boldsymbol{g}, \boldsymbol{e}_g, \phi_g) \tag{2}$$

where R is the rotation operator [19]: it compactly expresses the rigid rotation of, for instance, vector $\boldsymbol{p}$ about the axis marked by $\boldsymbol{e}_p$ by an angle ϕ_p as

$$\begin{aligned} \hat{\boldsymbol{p}}(\phi_p) &= R(\boldsymbol{p}, \boldsymbol{e}_p, \phi_p) \\ &= (\boldsymbol{p}\cdot\boldsymbol{e}_p)\boldsymbol{e}_p + \Big(\boldsymbol{p} - (\boldsymbol{p}\cdot\boldsymbol{e}_p)\boldsymbol{e}_p\Big)\cos\phi_p + \boldsymbol{e}_p \times \Big(\boldsymbol{p} - (\boldsymbol{p}\cdot\boldsymbol{e}_p)\boldsymbol{e}_p\Big)\sin\phi_p \end{aligned} \tag{3}$$

While the vector approach described in [19] is used here to facilitate physical insight, of course it is not the only viable method. Classical approaches based on homogeneous coordinates and 4×4 transformation matrices (widely used in [18]), or the twist exponential approach recently proposed in [20] can certainly be used to obtain the conjugate surface.

Getting back to the problem of calculating the pinion tooth surface that is conjugate to the gear tooth surface, the latter can be regarded as a tool that generates by envelope its conjugate pinion surface as the two members rotate about their axes according to the gear ratio. For a generic point $\boldsymbol{g}$ of the gear tooth surface to generate point $\boldsymbol{p}^{(c)}$ of the conjugate pinion, the equation of meshing must be satisfied and the following relation must hold (cf. Fig. 2)

$$\begin{aligned}\hat{\boldsymbol{g}}(\phi_g) &= \hat{\boldsymbol{p}}(\phi_p) + O_p - O_g \\ &= \hat{\boldsymbol{p}}(\phi_p) + \boldsymbol{d}_{gp}\end{aligned} \tag{4}$$

where

$$\boldsymbol{d}_{gp} := O_p - O_g = P\boldsymbol{e}_p + (d+E)\boldsymbol{e}_d - G\boldsymbol{e}_g \tag{5}$$

Note that d is negative if the system is right-handed (right-hand pinion, left-hand gear).

Turning the attention to the equation of meshing, the relative velocity between pinion and gear needs to be obtained. Let us first remark that rotation angles ϕ_p and ϕ_g are not independent quantities. In general, they are related to a *parameter of motion* ϕ. In the present case, one can let ϕ coincide with the gear rotation angle ϕ_g, i.e.

$$\phi_g(\phi) = \phi \tag{6}$$

$$\phi_p(\phi) = \tau\phi = \frac{N_g}{N_p}\phi \tag{7}$$

where the gear ratio τ is positive due to the sign convention adopted for ϕ_g and ϕ_p. The *geometric velocity* of a generic point on the pinion surface is (see also [19] for details)

$$\frac{d\hat{\boldsymbol{p}}(\phi_p(\phi))}{d\phi} = \frac{d\phi_p(\phi)}{d\phi}\boldsymbol{e}_p \times \hat{\boldsymbol{p}}(\phi_p(\phi)) \tag{8}$$

which, using Eqs. (4) and (7), becomes

$$\frac{d\hat{\boldsymbol{p}}(\phi_p(\phi))}{d\phi} = \tau\boldsymbol{e}_p \times \left(\hat{\boldsymbol{g}}(\phi) - \boldsymbol{d}_{gp}\right) \tag{9}$$

This geometric velocity is related to the ordinary velocity $d\hat{\boldsymbol{p}}/dt$ by

$$\frac{d\hat{\boldsymbol{p}}(t)}{dt} = \frac{d\hat{\boldsymbol{p}}(\phi_p(\phi))}{d\phi}\frac{d\phi(t)}{dt} = \tau\boldsymbol{e}_p \times \left(\hat{\boldsymbol{g}}(\phi) - \boldsymbol{d}_{gp}\right)\dot{\phi} \tag{10}$$

Similarly, the gear geometric velocity is

$$\frac{d\hat{\boldsymbol{g}}(\phi)}{d\phi} = \boldsymbol{e}_g \times \hat{\boldsymbol{g}}(\phi) \tag{11}$$

The *relative* geometric velocity of, say, the gear with respect to the pinion, denoted by $\hat{\boldsymbol{h}}_{gp}$, is given by

$$\begin{aligned}\hat{\boldsymbol{h}}_{gp}(\phi) &= \frac{d\hat{\boldsymbol{g}}(\phi)}{d\phi} - \frac{d\hat{\boldsymbol{p}}(\phi)}{d\phi} \\ &= \boldsymbol{e}_g \times \hat{\boldsymbol{g}}(\phi) - \tau \boldsymbol{e}_p \times \left(\hat{\boldsymbol{g}}(\phi) - \boldsymbol{d}_{gp}\right) \\ &= (\boldsymbol{e}_g - \tau \boldsymbol{e}_p) \times \hat{\boldsymbol{g}}(\phi) + \tau \boldsymbol{e}_p \times \boldsymbol{d}_{gp}\end{aligned} \tag{12}$$

At the generic conjugate pinion point being generated, the relative velocity must be orthogonal to the local contact normal (as per the equation of meshing). Such normal coincides with the (rotating) gear unit normal

$$\hat{\boldsymbol{n}}_g(\phi) = R(\boldsymbol{n}_g, \boldsymbol{e}_g, \phi) \tag{13}$$

Therefore, the equation of meshing can be expressed as

$$\hat{\boldsymbol{h}}_{gp}(\phi) \cdot \hat{\boldsymbol{n}}_g(\phi) = 0 \tag{14}$$

An even simpler form can be obtained by using the following property of the rotation operation (dot product property)

$$\hat{\boldsymbol{a}} \cdot \hat{\boldsymbol{b}} = R(\boldsymbol{a} \cdot \boldsymbol{b},\ \cdot\ ,\ \cdot\ ) \tag{15}$$

Indeed, applying a counter-rotation $-\phi$ around $\boldsymbol{e}_g$ to both vectors in Eq. (14)

$$R(\hat{\boldsymbol{h}}_{gp}(\phi), \boldsymbol{e}_g, -\phi) \cdot R(\hat{\boldsymbol{n}}_g(\phi), \boldsymbol{e}_g, -\phi) = 0 \tag{16}$$

and using relations (5) and (7) in [19, p. 615] one eventually obtains

$$\left[R(\boldsymbol{e}_g - \tau \boldsymbol{e}_p, \boldsymbol{e}_g, -\phi) \times \boldsymbol{g} + \tau R(\boldsymbol{e}_p \times \boldsymbol{d}_{gp}, \boldsymbol{e}_g, -\phi)\right] \cdot \boldsymbol{n}_g = 0 \tag{17}$$

or more compactly

$$\boldsymbol{h}_{gp}(\phi) \cdot \boldsymbol{n}_g = 0 \tag{18}$$

Here, unlike Eq. (14), the parameter of motion ϕ only appears in the first vector.

Solving the equation of meshing (18) (or (14)) for ϕ, one obtains the gear rotation angle $\phi^{(c)}$ at which the gear point $\hat{\boldsymbol{g}}$ generates its conjugate pinion counterpart

$$\hat{\boldsymbol{p}}^{(c)} = \hat{\boldsymbol{g}}(\phi^{(c)}) - \boldsymbol{d}_{gp} \tag{19}$$

In the fixed space, the point represented by position vector $\hat{\boldsymbol{p}}^{(c)}$, or equivalently by $\hat{\boldsymbol{g}}(\phi^{(c)})$, is a point of the *action surface* swept by the contact curves between the gear

tooth (the tool) and the conjugate pinion tooth being generated as they mesh [19, p. 625].

Finally, to obtain the corresponding point on the conjugate pinion tooth surface, position vector $\hat{\boldsymbol{p}}^{(c)}$ needs to be rotated back about the pinion axis, off the action surface, by the angle $-\phi_p^{(c)} = -\tau\phi^{(c)}$

$$\boldsymbol{p}^{(c)} = R(\hat{\boldsymbol{p}}^{(c)}, \boldsymbol{e}_p, -\tau\phi^{(c)}) \tag{20}$$

To perform computations, all vectors introduced so far can be expressed in just one fixed reference system, like system (x, y, z) shown in Fig. 2. Simple transformations are then required to express global vectors in the local pinion and gear reference frames.

2.3. Potential contact area

To specify ease-off topography, an area on the tooth surface is defined where contact can occur. Tooth surfaces are typically mapped to a two-dimensional domain (r, z) by circular projection of their points onto an axial plane (*projection plane*), that is a plane containing the gear/pinion axis. A generic point having coordinates (x_l, y_l, z_l) in the local (pinion or gear) reference frame is projected circularly onto the projection plane by the following bijective mapping

$$r_l = \sqrt{x_l^2 + y_l^2}, \qquad z_l = z_l \tag{21}$$

which is nothing but a circle coaxial with the pinion or the gear.

Let us consider a gear tooth flank generating its conjugate pinion flank, as done in section 2.2. The points forming the edges of the gear tooth (one of them being the flank root curve) would generate their conjugate counterparts as illustrated in Fig. 3(a), where they are shown on the pinion projection plane along with the region bounded by the pinion tooth edges. The area of intersection between the two regions is the pinion-based *potential contact area* (PCA). Obviously, the gear-based PCA (Fig. 3(b)) can be obtained by reversing the roles of pinion and gear. If the gear and the pinion were conjugate, the PCA would be covered with contact curves during meshing, whereas only part of it would come into contact if tooth surface modifications/errors were present. For these reasons, the PCA is in fact the largest possible area where contact can occur (the misalignments being fixed).

2.4. Ease-off and ease-off topography

Once a pinion-based or gear-based PCA has been obtained, the final step to defining ease-off topography is to discretize the PCA into a number of points, usually (but not

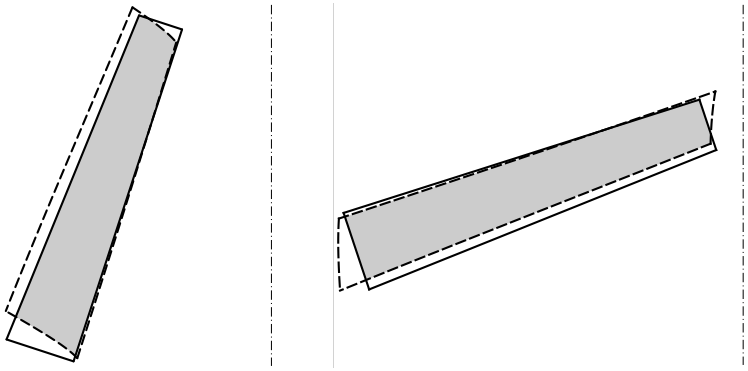

(a) Pinion-based PCA (shaded). Solid: pinion tooth edges. Dashed: conjugate pinion tooth edges (conjugate to the gear tooth edges).

(b) Gear-based PCA (shaded). Solid: gear tooth edges. Dashed: conjugate gear tooth edges (conjugate to the pinion tooth edges).

Figure 3: Potential contact areas.

necessarily) arranged as a rectangular grid. The grid points should lie slightly off the PCA borders to avoid issues associated with the vicinity of tooth edges.

In this work, the ultimate goal is to minimize the cumulative pinion deviations that alter the below defined pinion-based ease-off. The first step to calculating such ease-off is to determine the gear-based PCA (Fig. 3(b)), followed by discretization of the latter at a sufficiently representative number of points.

Let us draw upon the scenario and notation of section 2.2. Discretizing the gear-based PCA, each point sampled on it corresponds to a 3D point on the actual gear tooth surface represented by $\boldsymbol{g}_i$, and each gear tooth point $\boldsymbol{g}_i$ generates its conjugate pinion point $\boldsymbol{p}_i^{(\mathrm{c})}$ according to the process described in section 2.2. In the pinion local frame, point $\boldsymbol{p}_i^{(\mathrm{c})} = \left(x_{pi}^{(\mathrm{c})}, y_{pi}^{(\mathrm{c})}, z_{pi}^{(\mathrm{c})}\right)$ determines the circle having

$$r_{pi} = \sqrt{\left(x_{pi}^{(\mathrm{c})}\right)^2 + \left(y_{pi}^{(\mathrm{c})}\right)^2}, \qquad z_{pi} = z_{pi}^{(\mathrm{c})} \tag{22}$$

This circle can be used to sample the *designed* pinion tooth surface and obtain point $\boldsymbol{p}_i$. The ith *pinion-based ease-off value* e_{pi} is defined as the *angular distance* between points $\boldsymbol{p}_i^{(\mathrm{c})}$ and $\boldsymbol{p}_i$ induced by the circle (r_{pi}, z_{pi}) as shown in Fig. 4. The (pinion-based) ease-off topography is the set of all ease-off values calculated for each point of the PCA grid. An example is provided in Fig. 5. Typically, a rigid rotation is applied to the designed pinion surface so that all ease-off values are non-negative.

Alternatively, the same reasoning can be applied to obtain the gear-based ease-off topography by simply reversing the roles of pinion and gear. Derivation of a gear-based

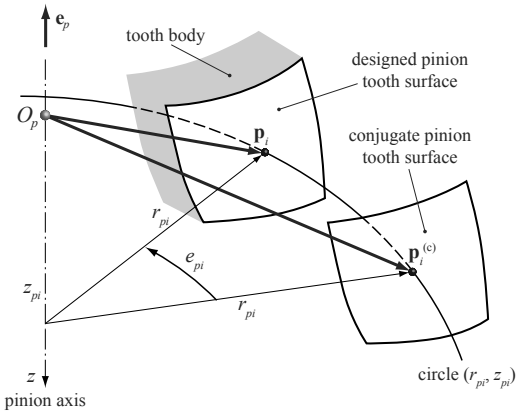

Figure 4: Definition of (pinion-based) ease-off, for one tooth side. Ease-off on the other tooth side is defined by analogy. A rigid rotation has been applied to the designed pinion surface in order to have non-negative ease-off everywhere.

ease-off topography is described in [21], where, however, ease-off is measured in linear units along the local surface normals.

The fact that ease-off measures how mismatched, i.e. non-conjugate, the pinion and gear tooth flanks are should now be evident. The role ease-off plays in affecting, or rather, dictating the tooth contact properties is demonstrated in [15, 16] (ease-off in linear units).

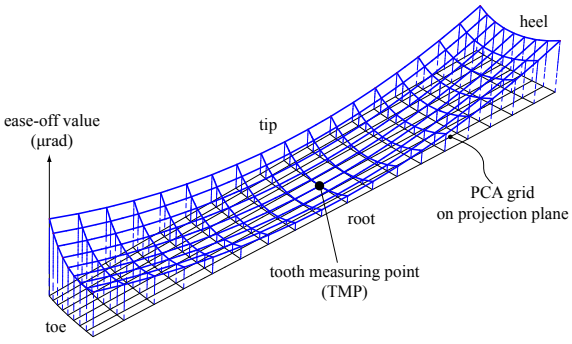

Figure 5: A typically designed shape for ease-off topography (zeroed at the TMP).

3. Surface and thickness deviations as ease-off variation

Deviations of the *real* cut/ground surface of the pinion and gear teeth from their theoretical (designed) models result in the actual ease-off topography being different from the designed one. Clearly, this has negative implications on contact properties, and eventually on accuracy, durability and noise rating of the gear drive. The present study aims to determine the machine-tool settings for recutting/regrinding the *pinion* teeth in order to reestablish the designed ease-off topography and the designed backlash.

A single pair of mating flanks (drive or coast) will be considered in the following. Treatment of the other pair is analogous.

3.1. Deviations of the real pinion tooth surface

Let us refer to Fig. 6, where a planar case is considered to facilitate understanding (but generalization to the spatial case is straightforward). We are assuming here that the gear tooth surface is perfect, that is the real surface coincides with the designed one. The figure represents a gear tooth generating the conjugate pinion tooth. In particular, point $\hat{P}_i^{(c)}$, which would be represented by position vector $\hat{\boldsymbol{p}}_i^{(c)}$ (not shown), is

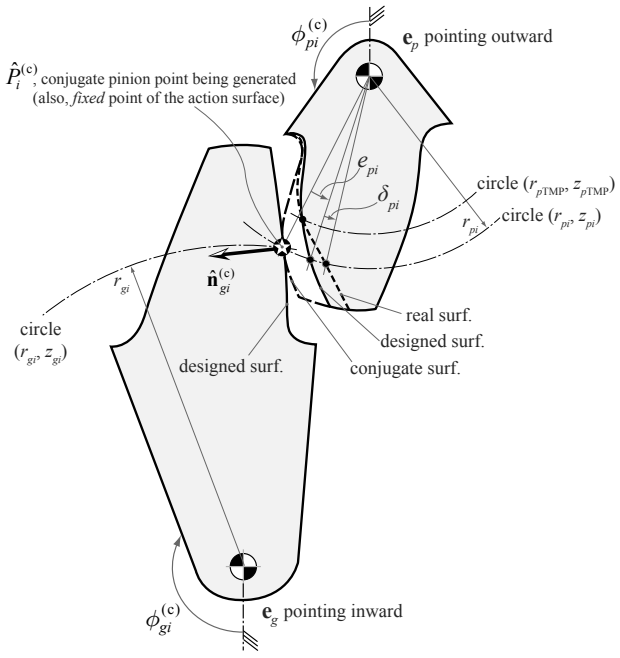

Figure 6: Pinion deviation and ease-off at a generic point.

being generated in the depicted scenario. (Please note once more that, in the present work, conjugacy indicates conjugate profiles of gear teeth whose transmission ratio is constant and equal to τ.) Point $\hat{P}_i^{(c)}$ (or $\hat{\boldsymbol{p}}_i^{(c)}$) determines the circle (r_{pi}, z_{pi}) that will be used for subsequent sampling of the pinion tooth surface. Besides the pinion's conjugate surface, Fig. 6 also shows its designed and real surfaces (exaggerated). The designed surface is assumed to be in the proper angular position to have non-negative ease-off, and e_{pi} is indeed the designed ease-off value obtained as described in section 2.4.

Regarding the real pinion tooth surface, the definition (and measurement) of surface deviations requires a proper orientation of the real surface with respect to the designed one. In the present study, the angular position of the real surface is chosen so that the deviation at the tooth measuring point (TMP, identified by the circle $(r_{p\mathrm{TMP}}, z_{p\mathrm{TMP}})$ in Fig. 6) is zero. This choice is fit for tooth thickness deviation to be easily accounted for, as will be detailed later. With the real and the designed surfaces thus *synchronized*, the pinion surface deviation at the *i*th point is obtained by sampling the two surfaces by the circle (r_{pi}, z_{pi}) and then measuring their *angular* offset δ_{pi} as shown in Fig. 6. Therefore, a positive/negative deviation corresponds to over-/underremoval of material. It is equally evident that tooth surface deviations defined this way directly result in ease-off deviations, and they eventually need to be minimized to restore the originally designed ease-off topography.

3.2. Key concept: gear surface deviations as equivalent pinion surface deviations

This section is devoted to presenting the key idea of this paper, namely to showing how surface deviations of the gear tooth can be mapped to *equivalent* surface deviations of the pinion tooth. The concept of equivalence is based here on the sameness of the resulting ease-off topography.

Let us pay close attention to Fig. 7(a), which elaborates on Fig. 6. This time the pinion is assumed to be perfect, while the real gear tooth surface deviates from the designed one. The *i*th angular deviation δ_{gi} is measured as shown in the figure (inward toward the interior of the tooth, as done for the pinion), after the real and the designed surfaces have been synchronized at the TMP (not represented).

Strictly speaking, the normal vector at the *i*th point G_i (with position vector $\boldsymbol{g}_i$) on the designed gear tooth surface differs from that at point $G_i^{(r)}$ on the real surface (obtained by piercing the latter by the circle (r_{gi}, z_{gi})). However, given the factual smoothness of the real surface and the magnitude of surface deviations, *it is reasonable*

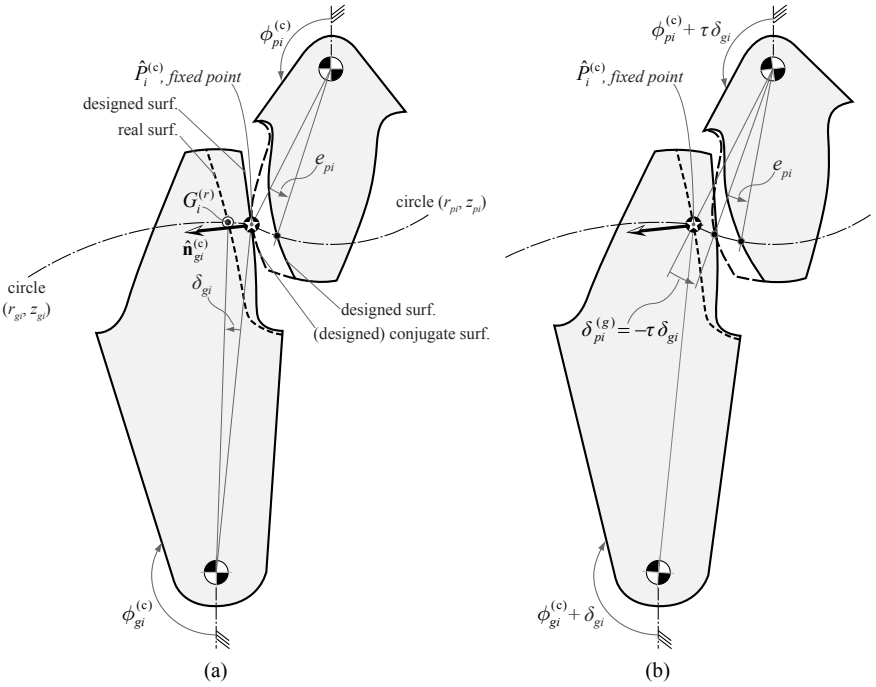

Figure 7: Gear deviations as equivalent pinion deviations.

to assume that the two normal vectors are collinear. Therefore, point $G_i^{(r)}$ will satisfy the equation of meshing and generate its conjugate point when it (or rather, $\hat{G}_i^{(r)}$, for the sake of rigor) occupies the same fixed space position as $\hat{P}_i{}^{(c)}$, represented by a starred symbol in Fig. 7 (and in Fig. 6). For this to happen, however, the gear must undergo an additional rotation equal to δ_{gi}, while the pinion rotates consequently by the additional angle $\tau\delta_{gi}$ (Fig. 7(b)). As a result, the designed ease-off e_{pi} undergoes a variation just equal to $\tau\delta_{gi}$. In other terms, such ease-off variation is nothing but a *gear-originated pinion deviation*

$$\delta_{pi}^{(g)} = \tau\delta_{gi} \tag{23}$$

Summarizing, the *real ease-off* $e_{pi}^{(r)}$, accounting for the presence of both pinion and gear deviations, but not as yet of tooth thickness deviation, is expressed by the simple relation

$$\begin{aligned} e_{pi}^{(r)} &= e_{pi} + \delta_{pi} + \delta_{pi}^{(g)} \\ &= e_{pi} + \delta_{pi} + \tau\delta_{gi} \\ &= e_{pi} + \delta_{pi} + \frac{N_g}{N_p}\delta_{gi} \end{aligned} \tag{24}$$

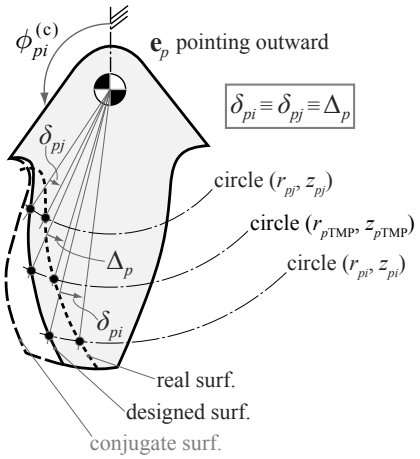

Figure 8: Pure tooth thickness deviation (pinion).

3.3. Tooth thickness deviation

Compensation of tooth thickness deviations is important not as much for mechanical strength of the tooth, which is relatively unaffected by micron-level surface variations, but rather for restoring the correct backlash. Thickness deviation of the pinion is usually compensated for by rotating the pinion blank by the angular thickness error. This simple approach can be used when the pinion is finished by a Fixed-Setting or Single-Side method. However, in the more restrictive case of the pinion and gear members being finished with a Spread-Blade or Completing method (both tooth sides cut simultaneously), tooth thickness deviation needs to be corrected through proper machine-tool setting variations. This is the approach taken in this work.

Figure 8 represents a pinion tooth whose real tooth surface has been obtained by simply rotating the designed surface around the pinion axis. This would be the effect induced by what is called here a *pure* tooth thickness deviation Δ_p, measured at the TMP and positive, for consistency, if the actual tooth thickness is smaller than the designed one, as in Fig. 8. All angular deviations have the same value Δ_p. Obviously, if the real and designed surfaces were synchronized at the TMP, deviations δ_{pi} would all be zero.

In sections 3.1 and 3.2, having synchronized the real and designed surfaces so as to have zero deviation at the TMP has been equivalent to assuming that the tooth thickness deviation is zero. In other words, deviations have been defined up to an arbitrary rigid rotation of the tooth surface around the pinion/gear axis. Now we dismiss such an

arbitrary rotation and replace it by the tooth thickness (angular) deviation. By doing so, the *total real ease-off* $E_{pi}^{(r)}$, accounting for the presence of both pinion and gear deviations as well as of their tooth thickness deviations, is expressed by

$$E_{pi}^{(r)} = e_{pi} + (\delta_{pi} + \Delta_p) + \tau(\delta_{gi} + \Delta_g) \tag{25}$$

Please note that tooth thickness deviation has to be factored in only once, i.e. for just one (either) pair of mating flanks, drive or coast.

4. Machine-tool setting corrections (for the pinion only)

The previous sections have been devoted to demonstrating how tooth surface and thickness deviations can be globally interpreted as *pinion-based ease-off deviations* δE_{pi} between the designed and the actual ease-off: they are given, at the ith point, by

$$\begin{aligned} \delta E_{pi} &= E_{pi}^{(r)} - e_{pi} \\ &= (\delta_{pi} + \Delta_p) + \tau(\delta_{gi} + \Delta_g) \\ &= (\delta_{pi} + \Delta_p) + \frac{N_g}{N_p}(\delta_{gi} + \Delta_g) \end{aligned} \tag{26}$$

which are nothing but equivalent pinion tooth surface deviations which now need to be minimized by identifying appropriate machine-tool setting corrections.

Minimizing deviations δE_{pi} (ideally, zeroing them) is the next step required to restore the originally designed ease-off topography, hence the theoretical contact properties of the gear drive. It is worth remarking once more that the method disclosed in this paper can reestablish the original ease-off topography by correcting the pinion only. The gear just needs to be measured, and it is "perfect as is".

4.1. Optimization problem formulation

The procedure for determining the machine-tool setting corrections for the pinion is an adaptation of the method proposed by the first two authors in [10] and recently in [14] for face-milled spiral bevel and hypoid gears, to which the reader is referred for details.

Let us consider Fig. 9. At a generic ith point, a deviation δE_{pi} is present. In order to compensate for such deviation, the method being proposed starts by imposing an equal and opposite angular deviation with respect to the originally designed tooth surface. The point thus determined (still belonging to the circle (r_{pi}, z_{pi})) is called *target point*. The set of all target points constitute the target surface. The aim here is to determine

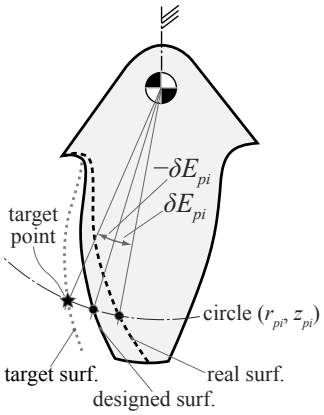

Figure 9: Definition of target point and target surface.

the machine-tool setting values $\boldsymbol{x}^{\star}$ required to generate the target surface, in an attempt to compensate for all deviations δE_{pi}.

It should be highlighted right away that this approach implicitly relies on the assumption that the mathematical model of the actual hypoid generator is affected by offset-type errors only, which is not true in general. However, the smallness of practical tooth surface deviations often legitimate the use of such assumption. When this is not the case, the proposed method may need to be applied more than once.

Figure 10 depicts three relevant tooth surfaces:

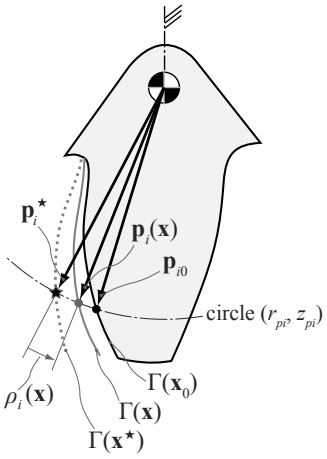

Figure 10: Definition of residual error.

- Surface $\Gamma(\boldsymbol{x}_0)$ is the designed surface, which should have been obtained by using the machine-tool settings values $\boldsymbol{x}_0$.

- Surface $\Gamma(\boldsymbol{x}^\star)$ is the target surface, to be obtained by the machine-tool setting values $\boldsymbol{x}^\star$, unknown as yet.

- Surface $\Gamma(\boldsymbol{x})$ can be regarded as the tooth surface generated by "generic" machine-tool setting values $\boldsymbol{x}$: it represents the tooth surface obtained at a certain iteration of the method being described.

For a generic grid point associated with the circle (r_{pi}, z_{pi}), its images on such three surfaces are represented by position vectors $\boldsymbol{p}_{i0}$, $\boldsymbol{p}_i^\star$ and $\boldsymbol{p}_i(\boldsymbol{x})$, respectively. Note that vector $\boldsymbol{p}_{i0}$ was simply referred to as $\boldsymbol{p}_i$ in the previous sections.

With reference to Fig. 10, the *residual error* $\rho_i(\boldsymbol{x})$ is defined here as the angular deviation between the target point $\boldsymbol{p}_i^\star$ and the point $\boldsymbol{p}_i(\boldsymbol{x})$ generated with current machine-tool setting values $\boldsymbol{x}$. The adjective "current" acquires a meaning later, when the solution method is considered. Extending this definition to all of the points (which, as a reminder, were originated by the gear-based PCA grid points), one obtains the *residual error vector*

$$\boldsymbol{\rho}(\boldsymbol{x}) = (\rho_1(\boldsymbol{x}), \rho_2(\boldsymbol{x}), \cdots, \rho_m(\boldsymbol{x})) \tag{27}$$

where m is the total number of points where measurements where taken at.

The solution to the problem of identifying the corrective machine-tool setting values can now be sought by solving the following nonlinear optimization (minimization) problem

$$\min_{\boldsymbol{x}} (\boldsymbol{\rho}(\boldsymbol{x}) \cdot \boldsymbol{\rho}(\boldsymbol{x})) = \min_{\boldsymbol{x}} \|\boldsymbol{\rho}(\boldsymbol{x})\|_2^2 \tag{28}$$

that is we are seeking the values $\boldsymbol{x}^\star$ that minimize the (squared) norm of the residual error vector $\boldsymbol{\rho}(\boldsymbol{x})$. Problem (28) is a *nonlinear least squares* (NLS) problem and, as amply discussed in [10, 14], it can be efficiently and accurately solved for $\boldsymbol{x}^\star$ by the iterative Levenberg-Marquardt method.

As to the choice of which machine-tool settings $\boldsymbol{x}$ to include as corrective design parameters, there are no theoretical restrictions. However, from a practical viewpoint, machine-tool setting changes that directly result in tooth depth variation (hence rootline shift) should be excluded. In particular, sliding base, machine-center-to-back, machine root angle, and their higher-order (UMC) coefficients should not be used.

For the sake of clarity, this correction procedure has been presented here for Fixed-Setting or Single-Side methods only. If a generating method is used that requires

double-flank compatibility, such as the Completing method, target points and surface of the other flank must be included as well, but the proposed procedure remains valid.

4.2. A remark about tooth depth deviation

Selecting corrective machine-tool settings that do not alter tooth depth is meaningful if tooth depth is not affected by errors in the first place. While it is often the case that slight tooth depth deviations can be disregarded, there may be situations in which they are unacceptable as they result in incorrect clearance (or even interference) between the tips of the teeth and the roots of the mating teeth.

To compensate for pinion tooth depth error, one could restore the nominal whole depth, hence the nominal clearance between gear tooth tip and pinion tooth root, by resorting to appropriate sliding base and/or machine-center-to-back and/or machine root angle adjustments, followed by recutting of the pinion prior to surface inspection and correction.

To compensate for gear tooth depth error, the nominal clearance between pinion tooth tip and gear tooth root would call for an analogous correction. Otherwise, to avoid recutting and remeasuring the gear, the nominal clearance could be reestablished by properly modifying the face angle and/or face apex of the pinion *blank*, but keeping in mind that this operation would affect the pinion tooth depth itself.

In the present work, tooth depth deviations, if any, are assumed to be allowable.

5. Numerical examples

The effectiveness of the proposed theoretical approach is demonstrated in this section. It was tested on a real face-milled hypoid gear set from an automotive application, whose basic design and manufacturing data are collected in Table 1. The proposed method was applied to the drive sides (pinion concave, gear convex). The finishing operation (grinding) was considered.

Some basic design machine-tool settings of the pinion and gear drive sides were purposely perturbed so as to simulate tooth surface and tooth thickness deviations. Coast sides were assumed to be perfect.

Tooth contact analysis (TCA) was used to assess the validity of the proposed method. In particular, contact pattern, contact pressure distribution, and motion transmission error were considered as evaluation parameters. TCA calculations were performed by the accurate commercial software package ANSol Hypoid Face Milled (HFM). The basic

Design parameter	Pinion		Gear
Number of teeth	11		41
Hand of spiral	Left		Right
Mean spiral angle (deg)	40.13		27.98
Pitch angle (deg)	18.12		71.50
Outer cone distance (mm)	108.66		112.41
Shaft offset (mm)		19.05	
Shaft angle (deg)		90.0	
Grinding method	Fixed-Setting	Face-milling	Spread-Blade
Generation type	Generated		Formate

Table 1: Basic design data of the hypoid gear set under consideration.

design TCA results, shown in Fig. 11, were obtained under a pinion torque of 5 Nm (to simulate unloaded TCA) and with zero (nominal) assembly errors.

5.1. Gear and pinion deviations

To simulate tooth surface and tooth thickness deviations of real teeth, the values of some nominal machine-tool settings were intentionally altered by quite sizable (arbitrary) variations, as shown in Table 2. The resulting tooth surface and tooth thickness deviations, calculated as described in the previous sections, are presented in Fig. 12. The initial gear-based PCA grid was composed of 19 points in the face direction and 9 points in the profile direction. The angular deviations are expressed in microradians (μrad), and the corresponding circular deviations, measured along the relevant

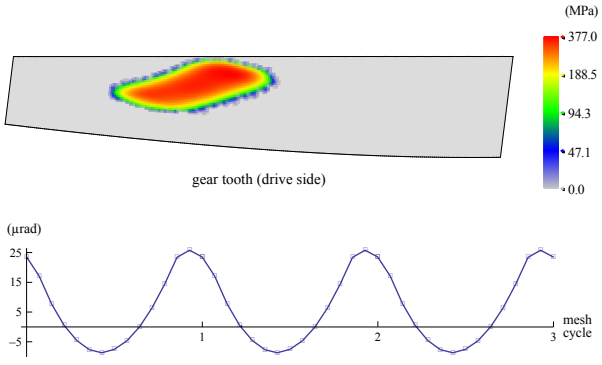

Figure 11: Nominal TCA results: loaded contact pattern (above) and pinion transmission error function (below). Maximum contact pressure: 377 MPa. Peak-to-peak transmission error: 34 μrad.

Machine-tool setting	Nominal	Perturbed	Variation
Pinion (concave side):			
grinding wheel pressure angle (deg)	12.000	11.600	−0.400
radial setting (mm)	81.700	81.720	+0.020
1st helical motion coeff. (mm/rad)	0.220	0.100	−0.120
Gear (convex side):			
grinding wheel radius (mm)	76.200	76.243	+0.043
grinding wheel point width (mm)	2.032	1.946	−0.086
vertical (mm)	78.377	78.350	−0.027

Table 2: Perturbations of selected machine-tool settings.

circles, are expressed in micrometers (μm) (in parentheses). Given the sign convention adopted, negative deviations correspond to insufficient material removal. The cumulative pinion deviations, i.e. what had been termed pinion-based ease-off deviations δE_{pi}

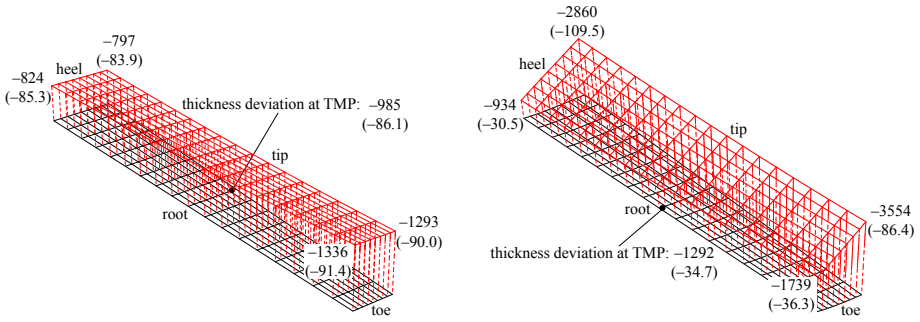

(a) Deviations ($\delta_{gi} + \Delta_g$) of the gear drive side.

(b) Deviations ($\delta_{pi} + \Delta_p$) of the pinion drive side.

Figure 12: Deviations of the gear and pinion drive sides, expressed in microradians (microns).

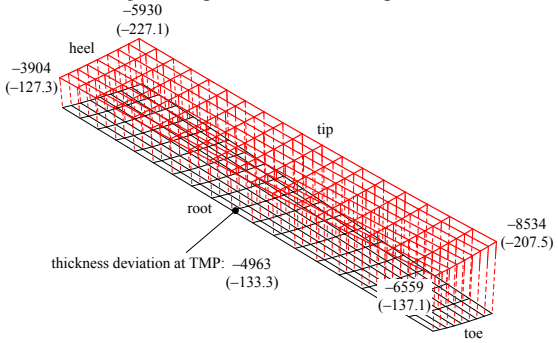

Figure 13: Cumulative deviations δE_{pi} of the pinion drive side.

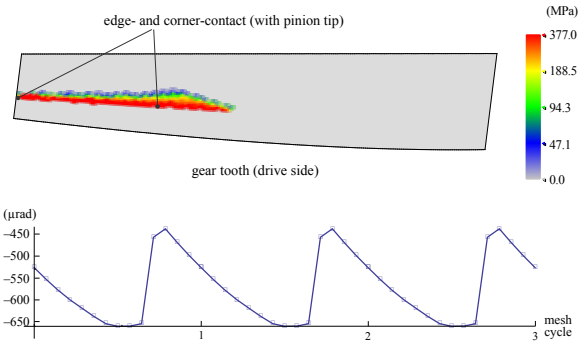

Figure 14: TCA results in the presence of the imposed deviations: loaded contact pattern (above) and pinion transmission error function (below). Maximum contact pressure: edge-/corner-contact (elastic estimate: 6457 MPa). Peak-to-peak transmission error: 222 μrad.

in section 4 (Eq. (26)), are shown in Fig. 13.

The corresponding TCA results, shown in Fig. 14, reveal that contact properties are dangerously degraded by the imposed surface deviations.

5.2. A preliminary test

A preliminary test was conducted to assess the correctness of the method in question. The three pinion machine-tool settings that had been perturbed to simulate the real pinion tooth surface (Table 2) were selected as design parameters, with the intent to determine their corrective variations that would compensate for the pinion deviations (those in Fig. 12(b)). By applying the method described in section 4, one would expect to obtain corrective variations very close and opposite to those in Table 2, although this is not the case in general, as problem (28) may have multiple global minima.

The variations actually obtained, shown in the last column of Table 3, resulted in a maximum residual error $\rho_i = 14$ μrad (absolute value), corresponding to a maximum circular deviation of just 0.5 μm. This demonstrates that the proposed approach is indeed headed in a promising direction.

Pinion machine-tool setting	Intentional variation	Calculated corrective variation
Grinding wheel pressure angle (deg)	−0.400	+0.397
Radial setting (mm)	+0.020	−0.020
1st helical motion coeff. (mm/rad)	−0.120	+0.105

Table 3: Intentional variations vs. calculated corrective variations of the three perturbed pinion machine-tool settings (for validation purposes).

5.3. Test 1: corrective machine-tool setting variations

The goal of Test 1 was to compensate for the pinion cumulative deviations in Fig. 13 by using a user-defined subset of machine settings and tool parameters. The initial values of the nine selected machine-tool settings and their corrective variations, calculated according to the method in section 4, are listed in Table 4. The modified roll polynomial was implemented as follows

$$\varphi(\beta) = R_a\left(\beta - \frac{2C}{2}\beta^2 - \frac{6D}{6}\beta^3 - \frac{24E}{24}\beta^4 - \frac{120F}{120}\beta^5\right) \tag{29}$$

where φ is the pinion rotation angle, β is the cradle rotation angle, and R_a is the ratio of roll.

The final residual error topography obtained using the corrective machine-tool settings is depicted in Fig. 15, where the residual errors are expressed in microradians and

Pinion machine-tool setting	Initial value	Calculated corrective variation
Grinding wheel radius (mm)	78.105	+0.128
Grinding wheel pressure angle (deg)	12.000	+0.344
Radial setting (mm)	81.700	−0.002
Cradle angle (deg)	70.470	+0.035
Ratio of roll	3.4905	+0.0023
Modified roll coeff. $2C$ (rad^{-1})	0.0000	+0.0010
Modified roll coeff. $6D$ (rad^{-2})	0.0000	−0.0057
Modified roll coeff. $24E$ (rad^{-3})	0.0000	+0.0030
Modified roll coeff. $120F$ (rad^{-4})	0.0000	+0.6000

Table 4: Test 1: corrective machine-tool setting variations.

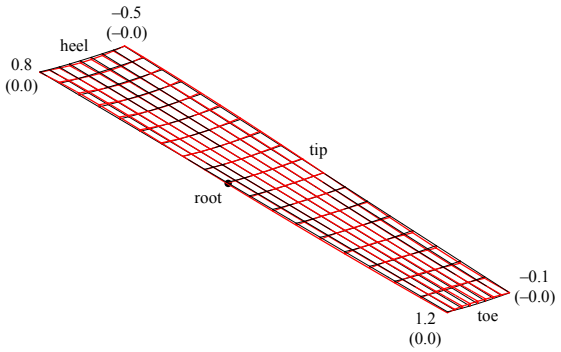

Figure 15: Test 1: residual error topography. Values are in microradians (microns). Maximum (absolute) value: 3 μrad (0.1 μm).

in microns (in parentheses, measured along the relevant circles). As this figure demonstrates, the correction process turned out to be practically perfect. The graphical TCA results virtually coincide with those in Fig. 11 and thus they are not shown here. The numerical TCA results are shown in the fourth column of Table 6.

5.4. Test 2: corrective machine setting variations

Test 2 was conceived to demonstrate that effective corrections can also be achieved using machine settings only, i.e. leaving the tool geometry unchanged (no need to redress the grinding wheel or to regrind the cutting blades). This profitable result is made possible through the complete flexibility provided by the correction method described in section 4. The initial values of the nine selected machine settings and their corrective variations are listed in Table 5.

Pinion machine setting	Initial value	Calculated corrective variation
Radial setting (mm)	81.700	−0.101
Cradle angle (deg)	70.470	−0.015
Tilt angle (deg)	18.200	−0.450
Swivel angle (deg)	−48.939	−0.124
Ratio of roll	3.4905	+0.0104
Modified roll coeff. $2C$ (rad^{-1})	0.0000	+0.0083
Modified roll coeff. $6D$ (rad^{-2})	0.0000	−0.0114
Modified roll coeff. $24E$ (rad^{-3})	0.0000	−0.0248
Modified roll coeff. $120F$ (rad^{-4})	0.0000	+0.5894

Table 5: Test 2: corrective machine setting variations.

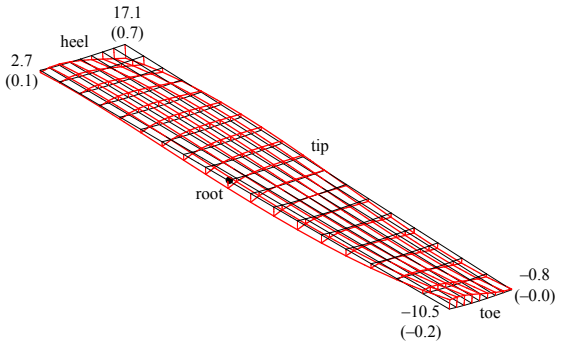

Figure 16: Test 2: residual error topography. Values are in microradians (microns). Maximum (absolute) value: 17 μrad (0.7 μm).

TCA evaluation parameter	Nominal	Perturbed	Test 1	Test 2
Maximum contact pressure (MPa)	377	edge-contact (6457)	375	374
Peak-to-peak transmission error (μrad)	34	222	34	36

Table 6: TCA results: Test 1 and Test 2 vs. nominal and perturbed designs.

The final residual error topography obtained using the calculated corrective settings is shown in Fig. 16, where the residual errors are expressed in microradians and in microns (in parentheses, measured along the relevant circles). The correction results are definitely good. Again, the graphical TCA results practically coincide with those in Fig. 11 and thus they are not shown. The numerical TCA results are shown in the fifth column of Table 6.

6. Conclusions

In this paper, a novel correction method aimed at compensating for tooth deviations of real spiral bevel and hypoid gears has been presented. Its distinctive features can be summarized as follows.

- Thanks to the definition and properties of ease-off, gear tooth surface and thickness deviations can be mapped into equivalent pinion deviations.
- Adding the gear-originated deviations to those of the pinion itself, the pinion eventually bears cumulative deviations, which have to be compensated for.
- Only the pinion needs to be corrected by minimizing such cumulative deviations, while the gear is perfect as it is.
- The employed correction process enables gear designers to select a user-specified number and type of machine-tool settings.

The numerical results have demonstrated that the proposed correction method can be very effective in restoring the originally designed contact properties, both when machine-tool settings and machine settings alone are used as corrective parameters. While the presented numerical examples involved grinding, this method can be applied both to cutting and grinding processes. Obviously, grinding guarantees a higher level of accuracy.

The proposed method has a number of remarkable advantages:

- An out-of-tolerance (ring) gear is not scrap metal anymore. It is a "perfect" gear. This becomes a great advantage for manufacturers who produce a very limited number of large gear sets, where each blank may easily cost tens of thousands of dollars.

- Neither a corrective machine-tool setting calculation nor a corrective machine-tool set-up is required for the gear. It just needs to be measured.

- When the gear is generated by a Spread-Blade method, or it is Formate, and the pinion is generated by a Single-Side or a Fixed-Setting method, the proposed approach is more accurate than ordinary practice, in that the gear flanks are indirectly corrected as if they had been independently generated.

- Errors introduced during the correction stage of the gear are eliminated, which adds to the final level of accuracy.

Finally, let us highlight another possible and technically interesting application of the ideas presented in this paper. Prior to grinding, gear sets are often heat treated to increase their tooth surface hardness. Depending on the size and shape of the two members, there exist cases in which heat treatment induces relatively large tooth distortions. Therefore, subsequent stock removal by grinding results in the case depth not being uniform beneath the surface, thereby reducing tooth surface hardness and strength at some locations. The proposed method can be extended to balance grinding stock removal. In particular, the gear and the pinion could be ground (after case hardening) in such a way to distribute case depth more evenly below the tooth surfaces of both members, while concurrently maintaining the designed ease-off topography, hence the designed contact properties.

References

[1] T. J. Krenzer, R. Knebel, Computer aided inspection of bevel and hypoid gears, SAE Paper 831266, International Off-Highway Meeting, Milwaukee, WI, 1983.

[2] T. J. Krenzer, Computer aided corrective machine settings for manufacturing bevel and hypoid gear sets, AGMA Paper 84FTM4, Fall Technical Meeting, Washington, DC, 1984.

[3] F. L. Litvin, Y. Zhang, J. Kieffer, R. F. Handschuh, Identification and minimization of deviations of real gear tooth surfaces, J. Mech. Des. 113 (1991) 55–62.

[4] F. L. Litvin, C. Kuan, J. C. Wang, R. F. Handschuh, J. Masseth, N. Maruyama, Minimization of deviations of gear real tooth surfaces determined by coordinate measurements, J. Mech. Des. 115 (1993) 995–1001.

[5] H. J. Stadtfeld, Handbook of Bevel and Hypoid Gears, Rochester Institute of Technology, Rochester, NY, USA, 1993.

[6] C.-Y. Lin, C.-B. Tsay, Z.-H. Fong, Computer-aided manufacturing of spiral bevel and hypoid gears with minimum surface deviation, Mech. Mach. Theory 33 (1998) 785–803.

[7] C. Gosselin, T. Nonaka, Y. Shiono, A. Kubo, T. Tatsuno, Identification of the machine settings of real hypoid gear tooth surface, J. Mech. Des. 120 (1998) 429–440.

[8] C.-Y. Lin, C.-B. Tsay, Z.-H. Fong, Computer-aided manufacturing of spiral bevel and hypoid gears by applying optimization techniques, J. Mater. Process. Tech. 114 (2001) 22–35.

[9] Y.-P. Shih, Z.-H. Fong, Flank correction for spiral bevel and hypoid gears on a six-axis CNC hypoid generator, J. Mech. Des. 130 (2008) 062604.

[10] A. Artoni, M. Gabiccini, M. Guiggiani, Nonlinear identification of machine settings for flank form modifications in hypoid gears, J. Mech. Des. 130 (2008) 112602.

[11] Q. Fan, Higher-order tooth flank form error correction for face-milled spiral bevel and hypoid gears, J. Mech. Des. 130 (2008) 072601.

[12] Q. Fan, Tooth surface error correction for face-hobbed hypoid gears, J. Mech. Des. 132 (2010) 011004.

[13] A. Guenther, Interpretation of bevel gear topography measurements, CIRP Ann-Manuf. Techn. 60 (2011) 551–554.

[14] M. Gabiccini, A. Artoni, M. Guiggiani, On the identification of machine settings for gear surface topography corrections, J. Mech. Des. 134 (2012) 041004.

[15] M. Kolivand, A. Kahraman, A load distribution model for hypoid gears using ease-off topography and shell theory, Mech. Mach. Theory 44 (2009) 1848–1865.

[16] M. Kolivand, A. Kahraman, An ease-off based method for loaded tooth contact analysis of hypoid gears having local and global surface deviations, J. Mech. Des. 132 (2010) 071004.

[17] ANSI/AGMA 2005–D03, Design Manual for Bevel Gears, American Gear Manufacturers Association, 500 Montgomery Street, Suite 350, Alexandria, VA, USA, 2003.

[18] F. L. Litvin, A. Fuentes, Gear Geometry and Applied Theory, 2nd edition, Cambridge University Press, New York, NY, USA, 2004.

[19] F. D. Puccio, M. Gabiccini, M. Guiggiani, Alternative formulation of the theory of gearing, Mech. Mach. Theory 40 (2005) 613–637.

[20] M. Gabiccini, A twist exponential approach to gear generation with general spatial motions, Mech. Mach. Theory 44 (2008) 382–400.

[21] Y.-P. Shih, Z.-H. Fong, Flank modification methodology for face-hobbing hypoid gears based on ease-off topography, J. Mech. Des. 129 (2007) 1294–1302.